New Journal of Physics
The open access journal at the forefront of physics

Deutsche Physikalische Gesellschaft DPG IOP Institute of Physics

PAPER • OPEN ACCESS

Ballistic phonon lensing by the non-planar interfaces of embedded nanoparticles

To cite this article: Theodore Maranets and Yan Wang 2023 *New J. Phys.* **25** 103038

View the article online for updates and enhancements.

This content was downloaded from IP address 68.6.85.124 on 20/10/2023 at 18:58

IOP Publishing New J. Phys. 25 (2023) 103038 https://doi.org/10.1088/1367-2630/ad025a

New Journal of Physics
The open access journal at the forefront of physics

Deutsche Physikalische Gesellschaft DPG
IOP Institute of Physics

Published in partnership with: Deutsche Physikalische Gesellschaft and the Institute of Physics

OPEN ACCESS

RECEIVED
14 August 2023

REVISED
28 September 2023

ACCEPTED FOR PUBLICATION
11 October 2023

PUBLISHED
20 October 2023

Original Content from this work may be used under the terms of the Creative Commons Attribution 4.0 licence.

Any further distribution of this work must maintain attribution to the author(s) and the title of the work, journal citation and DOI.

PAPER

Ballistic phonon lensing by the non-planar interfaces of embedded nanoparticles

Theodore Maranets and Yan Wang*

Department of Mechanical Engineering, University of Nevada, Reno, NV 89557, United States of America
* Author to whom any correspondence should be addressed.

E-mail: yanwang@unr.edu

Keywords: phonon transport, interfaces, nanoparticle, molecular dynamics

Abstract

In this work, we investigate the scattering behavior of a ballistic phonon wave incident on a dopant spherical nanoparticle embedded within a pure crystal through molecular dynamics simulations. Unique to this work, we also conduct conjugate simulations of ballistic phonon scattering on a dopant thin slab to compare and contrast scattering by non-planar heterogeneous interfaces (nanoparticle) and planar heterogeneous interfaces (thin slab). Analysis of the wave dynamics in real and reciprocal spaces reveal phonon mode-conversion in the nanoparticle scattering system is due to an unreported 'phonon lensing' effect where the phonon wave propagation is altered by refraction and reflection through the non-planar interfaces of the nanoparticle. The specific states of mode-conversion is shown to change with the character of the lensing that varies with nanoparticle size. Most significantly, the lensing phenomenon is absent in the phonon scattering by the thin slab and consequentially, results in differences in the scattering behaviors between the planar and non-planar interfaces.

1. Introduction

Strong reduction of thermo-electronic device dimensions in recent years has yielded high densities of heterogeneous interfaces at nano-meter length scales. As such, proper estimation of lattice heat transfer across nano-scale interfaces is critical for improved design of miniaturized devices in thermal applications such as thermal interface materials, thermoelectric materials, and phase change memory devices [1]. Detailed in other works, computation of the heat current across the interface of two materials requires evaluation of a mode and wave-vector-dependent phonon transmission function $\mathcal{T}(p,\boldsymbol{k})$ that quantifies the probability of a phonon mode p with wave-vector $\boldsymbol{k}$ scattering in a particular direction [2]. Modeling of $\mathcal{T}(p,\boldsymbol{k})$ has been a key problem in contemporary analyses of interfacial phonon transport.

Early solutions to $\mathcal{T}(p,\boldsymbol{k})$ include the acoustic mismatch model (AMM) which treats phonons as acoustic waves that reflect and transmit at a continuous solid–solid boundary in a specular fashion (figure 1(a)) [3]. Typically, the specular assumption is reasonable when the interface is perfectly smooth or the surface roughness is much less than the critical phonon wavelength. However, even at low temperatures, when the phonon spectrum is concentrated to long wavelengths, the AMM is a poor descriptor due to the impact of surface roughness [4]. Considering the nonideal interface, Swarz and Pohl proposed the diffuse mismatch model (DMM) that models the phonon reflection and transmission as entirely diffuse, independent of the angle of incidence (figure 1(b)) [3]. The formulations of $\mathcal{T}(p,\boldsymbol{k})$ for both AMM and DMM assume elastic phonon scattering at the interface. Such assumption is found to be untrue as inelastic-phonon transmission and interface mode conversion is observed at finite temperatures [5, 6]. Variations of the AMM and DMM have been developed to improve accuracy and applicability while other works applying computational methods such as lattice dynamics, molecular dynamics (MD), and atomistic Green's function have been made to better understand interfacial phonon transport in regards to $\mathcal{T}(p,\boldsymbol{k})$ [2].

Much attention has been paid to calculation of phonon reflection and transmission at solid-solid interfaces with a plethora of material combinations studied, however, in these studies, interfaces examined

© 2023 The Author(s). Published by IOP Publishing Ltd on behalf of the Institute of Physics and Deutsche Physikalische Gesellschaft

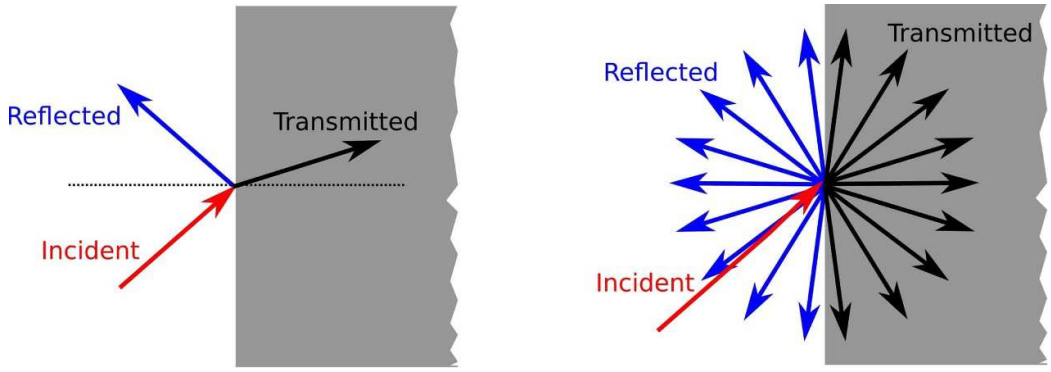

(a) Acoustic Mismatch Model (AMM) (b) Diffuse Mismatch Model (DMM)

Figure 1. The AMM and DMM evaluations of $\mathcal{T}(p,\mathbf{k})$. The AMM assumes specular interface scattering while the DMM treats the interaction as entirely diffuse.

have been planar or approximately planar (e.g. planar interfaces with engineered surface roughness and/or nano-structures such as those examined by Xie *et al* [7]). Surprisingly little effort has been made as of yet to understand phonon transport across interfaces with significant non-planar geometry. Moreover, to our knowledge, no work in the literature has been made to find a relationship between phonon scattering at planar and non-planar interfaces. Addressing such question would progress development of a holistic theory of interfacial phonon transport, instead of treating phonon scattering at planar and non-planar interfaces separately.

1.1. Nanoparticle

1.1.1. Experiment

Understanding phonon scattering at non-planar interfaces is notably relevant to analysis of lattice heat transfer through embedded nanoparticles, nano-scale sized dopant particulates embedded within a host lattice. A nanoparticle can be viewed as a combination of two non-planar heterogeneous interfaces that in addition to reflection and transmission, can induce phonon wave-trapping, localization, and lagged dissipation effects. Several experimental works have demonstrated embedded nanoparticles can manipulate thermal transport in a variety of crystalline solids [8–10]. Analyses of experimental results have generally been limited to case-by-case bases; implementing application-specific theories or first-principles calculations. Few theoretical (both analytical and computational) efforts have been made to provide a general description of phonon-nanoparticle scattering that can cohesively explain the various reported thermal transport phenomena in nanoparticle-laden materials. The merits and short-comings of these theories and how the research detailed in this report is motivated, will now be discussed.

1.1.2. Analytical theory

Majumdar first proposed that the scattering behavior of a phonon incident on a lattice imperfection is similar to the scattering of electromagnetic waves by small particles [11]. Under this analogy, the expression for the scattering cross-section for phonons incident on a spherical nanoparticle was formulated as

$$C^{-1}_{\text{nanoparticle}} = C^{-1}_{\text{Rayleigh}} + C^{-1}_{\text{Geometric}} = \left\{ \frac{4}{9}\pi R^2 \left(\frac{\Delta\rho}{\rho} \right)^2 (kR)^4 \right\}^{-1} + \left\{ 2\pi R^2 \right\}^{-1} \tag{1}$$

where R is the radius of the nanoparticle, ρ is the density of the host material and $\Delta\rho$ is the density difference between the host and impurity materials [12]. This model was developed through perturbation theory while heavily borrowing relationships from light scattering theory. While effective for simple calculation, two key flaws in the equation are immediately present which hinders its accuracy. The model is not mode-resolved and wavelength dependent behavior is poorly described by a 'patching' of the scattering relations for the Rayleigh regime ($\lambda \gg R$) and Geometric regime ($\lambda \ll R$), thus omitting details of the Mie scattering regime ($\lambda \approx R$). These flaws have motivated development of alternative models to characterize the complexity of phonon-nanoparticle scattering.

Another prominent analytical solution is the treatment of phonons as acoustic waves. Works such as Prasher [13] and Feser [14] have applied the existing scattering cross-section expressions of plane harmonic longitudinal (compression) and transverse (shear) waves, respectively by an elastic sphere in an isotropic

elastic solid to model thermal conductivity of nanoparticle-laden composites. The acoustic analogy provides wave-vector and mode-specific cross-sections which are unattainable by the electromagnetic wave analogy, however, the approach is realistically limited to systems like the nanoparticle-in-alloy composite where low-frequency phonons, whose dispersion is approximately linear and thus well described by acoustic wave theory, predominate thermal transport. The acoustic analogy is not expected to be accurate when the higher frequencies, whose dispersion is non-linear, have a non-negligible contribution to the thermal conductivity. Furthermore, a continuum theory assumes no thermal transport by optical phonons. First-principles calculations have revealed such assumption can be inaccurate for thermal conductivities of nano-structured materials [15].

Further first-principles analyses of phonon-nanoparticle scattering include the atomistic Green's function approach by Kundu *et al* [16] In the parameter-free calculation, the perturbation matrix is solely formed by the mass difference as the influence of the elastic contrast is taken to be negligible compared to the mass difference. A virtual crystal approximation is assumed, and the total mode-wise phonon-nanoparticle scattering rate, considering independent scatterers in a homogeneous medium, is evaluated. Thermal conductivities of $Si_{0.5}Ge_{0.5}$ alloys with embedded nanoparticles are subsequently calculated with and without the Born approximation.

The common factor in all the analytical solutions discussed, borrowing from various first-principles methods and theories, is the evaluation of a scattering rate expression to describe the ultimate effect of nanoparticles on phonon heat conduction. Minimal details if not any of the lattice wave scattering dynamics, such as scattering phase functions, phonon mode-conversion, and localization behaviors, have been provided by existing analytical works, often for the sake of mathematical tractability. These effects can significantly influence thermal transport and so must be properly considered. For instance, in composites with high volume fractions of embedded nanoparticles, the distances between nanoparticles become comparable to the phonon wavelengths. It is expected in this case, that an independent scattering approximation (phonons solely scatter off of a single nanoparticle in its phonon lifetime), assumed in many first-principles analyses, becomes invalid. Descriptions of a scattering-phase function and the nanoparticle effect on mean free path would be necessary to evaluate the multiple and dependent phonon scattering dynamics that would dictate thermal transport. As a consequence of the limitations of analytical approaches, several computational studies, with fewer simplifying assumptions, have been developed to more rigorously investigate phonon-nanoparticle interactions.

1.1.3. Computational theory

Computational analyses of phonon scattering by embedded nanoparticles have leaned towards atomistic methods. Zuckerman and Lukes, in particular, applied the MD based phonon wave-packet method to study how incident acoustic phonon wave-packets, propagating in the [100] direction of a Lennard–Jones (LJ) FCC crystal, interacted with a nanometer-sized scatterer [17]. Scattering phase functions for the longitudinal and summed-transverse modes were computed and compared to the analytical solutions of acoustic wave scattering by a spherical obstacle. Strong disagreement was found and was attributed to the anisotropic and discrete nature of the lattice. Simulations were also conducted with geometrically different scatterers (e.g. spherical nanoparticle vs cubic-shaped nanoparticle) and variation in the phase functions were observed, however, minimal discussion was made to explain why scattering differed when, effectively, the non-planar interface of the nanoparticle was changed. Ultimately the question as to why different shaped nanoparticles (with different sizes in proportion to the incident phonon wavelength) yielded differences in the phonon scattering behavior was unanswered. This question is fundamentally linked to understanding the connection between phonon scattering at planar and non-planar interfaces.

Motivated by the shortcomings of Zuckerman and Lukes as well as some specific limitations of the wave-packet method, Kakodkar and Feser applied the frequency domain perfectly matched layer (FDPML) method to study phonon-nanoparticle scattering with exact wave-vector and mode resolution [18]. A perfectly matched layer allows numerical calculation of the wave dynamics of a scattering system (i.e. the local space surrounding and including the nanoparticle) within a reduced computational region. By modeling the dynamics equations in the frequency domain, the FDPML becomes a quasi-lattice dynamics approach in which the phonon properties, particularly dispersion and scattering efficiencies, of the scattering system are effectively evaluated over the entire Brillouin zone [19]. New details elucidated by the FDPML technique include scattering efficiencies of optical phonons, which the MD based wave-packet method, and both acoustic and electromagnetic analytical analogies are unable to capture. The main flaw with the FDPML technique, like that of lattice dynamics calculations, is that details of the phonon wave scattering (an inherently transient process) in time and real space are hidden. MD, through explicit modeling of the lattice vibrational modes, naturally allows observation of the wave scattering in both real and reciprocal spaces and both time and frequency domains [20]. Access to a variety of analysis tools makes MD most malleable and

capable in computing broad phonon properties like scattering efficiencies and phase functions while simultaneously studying the fundamental wave dynamics (reflection, transmission, and absorption behavior) that affect such properties.

1.2. Objective

In this work, the MD based wave-packet method is revisited to rigorously investigate ballistic acoustic phonon wave scattering by a spherical nanoparticle at the atomistic level. Unique to this work, identical simulations of the phonon wave incident on a thin slab, which can be considered as a junction of two planar heterogeneous interfaces (whereas the nanoparticle is non-planar), are also conducted. Computational analyses of the phonon scattering in both real and reciprocal spaces are made and the respective results from the nanoparticle and thin slab scattering systems are compared to quantify the effect of interfacial geometry on phonon wave transport. A distinguishing effect of ballistic phonon scattering at the non-planar interfaces of the nanoparticle, an unreported phenomena we term 'phonon lensing' is uncovered and shown to significantly influence the states of mode conversion in the scattering system.

2. Methodology

MD modeling of phonons as propagating wave-packets that can interact with each other or heterogeneous structures is a powerful tool for direct phonon scattering analyses as the wave-packet captures key phonon properties such as mode, wavelength, group velocity, relaxation time, and coherence length [21]. The method applied in this work is based off the technique developed in Schelling *et al* [22]. We chose a LJ FCC structure as our model material system for reduced computational cost. The LJ model for interatomic interactions is given as

$$\phi_{ij}\left(r_{ij}\right) = 4\epsilon\left[\left(\frac{\sigma}{r_{ij}}\right)^{12} - \left(\frac{\sigma}{r_{ij}}\right)^{6}\right]. \tag{2}$$

The host matrix has a molecular weight of 40 g mol^{-1}, approximately the weight of solid argon, while the nanoparticle matrix has a molecular weight of 90 g mol^{-1}. The parameter set of $\epsilon_{Ar} = 0.0104$ eV, $\sigma_{Ar} = 0.34$ nm, and a cutoff radius of $2.5\sigma_{Ar}$ has been used in previous studies on LJ-modeled solid argon [23, 24]. In this work, we use $\epsilon = 16\epsilon_{Ar}$ for the interactions of all atom types to mimic stronger bonded materials such as Si/Ge and GaAs/AlAs as done in previous LJ-based MD investigations [25, 26]. We forgo inclusion of an elastic contrast as it is an added degree of complexity to the scattering system and impurity scattering is shown to be primarily due to the mass contrast [27]. The relaxed lattice constant determined MD relaxation commands for the given model material was $a = 5.2686$ Å.

The wave-packet simulations are conducted in the following process. First, a phonon mode p and select wave-vector $\boldsymbol{k} = \left[k_x, k_y, k_z\right] = \left[k_0, 0, 0\right]$ to which the wave-packet will be centered at in reciprocal space is chosen from the zero-temperature [100] phonon dispersion. To minimize the influence of changes in relative coherence length i.e. to solely focus on examining how scattering differs when the proportion of the nanoparticle size to the phonon wavelength is altered, the real-space spatial width ξ of the wave-packet, which is analogous to the phonon coherence length, is scaled to according to the center phonon wavelength $\lambda_0 = \frac{2\pi}{k_0}$ and lattice constant a in the following fashion

$$\xi_{UC} = \left\lceil \frac{30\lambda_0}{a} \right\rceil, \quad \xi = \xi_{UC} a \tag{3}$$

where $\lceil \cdot \rceil$ is the ceiling function. The reasoning for the inclusion of a large multitude of periods in the wave-packet will now be given. The spatial width ξ in real space is inversely proportional to the spatial width of the phonon wave-packet in reciprocal space. Improving the wave-vector accuracy involves a narrowing of the signal spread about k_0 i.e. ξ must be lengthened. Phonons with large wave-vectors possess low wavelengths, therefore to generate a phonon wave-packet centered at a large k_0 with a sufficiently narrow spread in reciprocal space, a large number of periods is required for the wave-packet signal in real-space. Since the number of periods in the wave-packets simulated is kept fixed to ensure wave-packet consistency in different simulations, ξ increases as λ_0 increases and so the spatial width of the signal in reciprocal space further narrows, increasing the wave-vector accuracy of the simulation as k_0 is decreased.

The length of the simulation domain on the x axis, aligned along the [100] direction, is set to $L_x = 20\xi$ and the time duration of the simulation is controlled such that the Gaussian crest of the wave-packet i.e. the real space center would approximately travel (with group velocity $v_{g0} = v_g(p, k_0)$) from $0.3L_x$ to $0.8L_x$ if there were no scatterer present. Such scaling in real space and the time domain provides further consistency

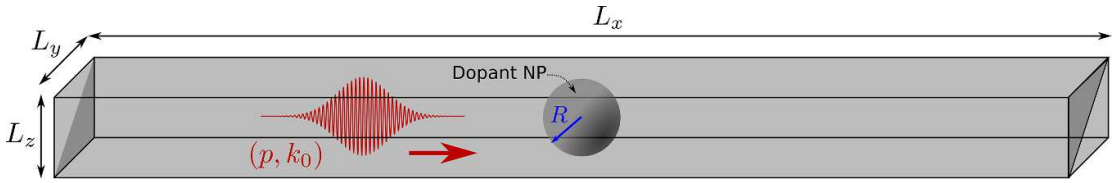

Figure 2. System diagram of the molecular dynamics phonon wave-packet method.

between different simulations. The wave-packet is generated at the beginning of the MD simulation by applying the following equations for atom displacement and velocity.

$$u_{i,m} = A_i \varepsilon_{p,k_0,i} \exp\left(i[k_0 \cdot (x_m - x_0) - \omega_0 t]\right) \exp\left(-(x_m - x_0 - v_{g0} t)^2 / \xi^2\right) \tag{4}$$

$$v_{i,m} = \frac{\partial u_{i,m}}{\partial t} \tag{5}$$

where the real parts of $u_{i,m}(t=0)$ and $v_{i,m}(t=0)$ are the initial displacement and velocity for the ith atom in the mth unit cell, respectively. A_i is a user-defined amplitude, $\varepsilon_{p,k_0,i}$ is the eigenvector, $\omega_0 = \omega(p, k_0)$ is the center phonon frequency, x_m is the position of the mth unit cell, and $x_0 = 0.3L_x$ is the chosen initial position of the Gaussian crest. Phonon properties are determined from lattice dynamics calculations. A_i controls the amplitude of atomic vibration and is kept to a low value ($\approx 10^{-4}a - 10^{-5}a$) depending on the magnitude of ω_0 to ensure no anharmonic interactions between neighboring atoms that would break the coherence of the wave-packet and thus ruin the simulation of a ballistic phonon.

A diagram of the nanoparticle simulation domain is presented in figure 2. The single nanoparticle with radius R is placed at $x = 0.5L_x$ in the center of the yz cross-section. The y and z dimension lengths are equal and scaled such that the cross-sectional area is approximately 3 times the projected area of the spherical nanoparticle. In the thin slab simulations, the thin slab is located at $x = 0.5L_x$ and the thin slab interface spans the entire cross-section. From preliminary tests, the phonon wave-packet scattering with the thin slab was not observed to vary with cross-sectional area, so in all thin slab simulations, the y and z dimension lengths were set to $L_y = L_z = 4a$ for reduced computational cost. Similar to scattering analyses of light waves by small particles, simulations for both nanoparticle and thin slab cases are distinguished by phonon mode p and a size factor γ defined as the following expression.

$$\gamma = \frac{R}{\lambda_0}. \tag{6}$$

Varying γ for a particular p involved changing λ_0 and/or R. Thus, based on the criteria detailed in this section, the simulation domain would be regenerated for each γ. Since the nanoparticle matrix possesses a lower phonon dispersion than the host material, the selection of k_0 (the initial wave-packet is generated in the host material) is made such that there is always a non-zero transmission of ω_0 from the host material to the dopant nanoparticle.

After the phonon wave-packet is generated at the start of the simulation, the simulation is run in a micro-canonical ensemble: conserving particle count, volume, and energy. Periodic boundary conditions are applied to all three dimensions. The LAMMPS software was used to implement the MD simulations [28].

3. Results

Scattering simulations of several size factors varying from $\gamma = 0.15$ (Rayleigh Regime) to $\gamma = 10$ (Geometric regime) for all three acoustic modes were conducted. For the sake of brevity, mostly the LA and TA1 results for size factors of $\gamma = [0.15, 0.5, 1.0, 2.0, 10.0]$ will be discussed as the scattering behaviors of the TA1 and TA2 modes were nearly equivalent along their respective polarization directions.

3.1. Scattered waveforms

3.1.1. Introduction

The scattering dynamics is first studied in real-space along the path of propagation of the initial wave-packet to examine the discrete effect of the scatterer on the phonon reflection and transmission as exemplified in figure 3. The scattering behaviors of both the nanoparticle and thin slab varies with γ and the comparison between the nanoparticle scattering and conjugate thin slab simulation is also observed to change. The waveforms of the LA, TA1, and TA2 velocities (color-coded) at the end of the simulation duration are plotted

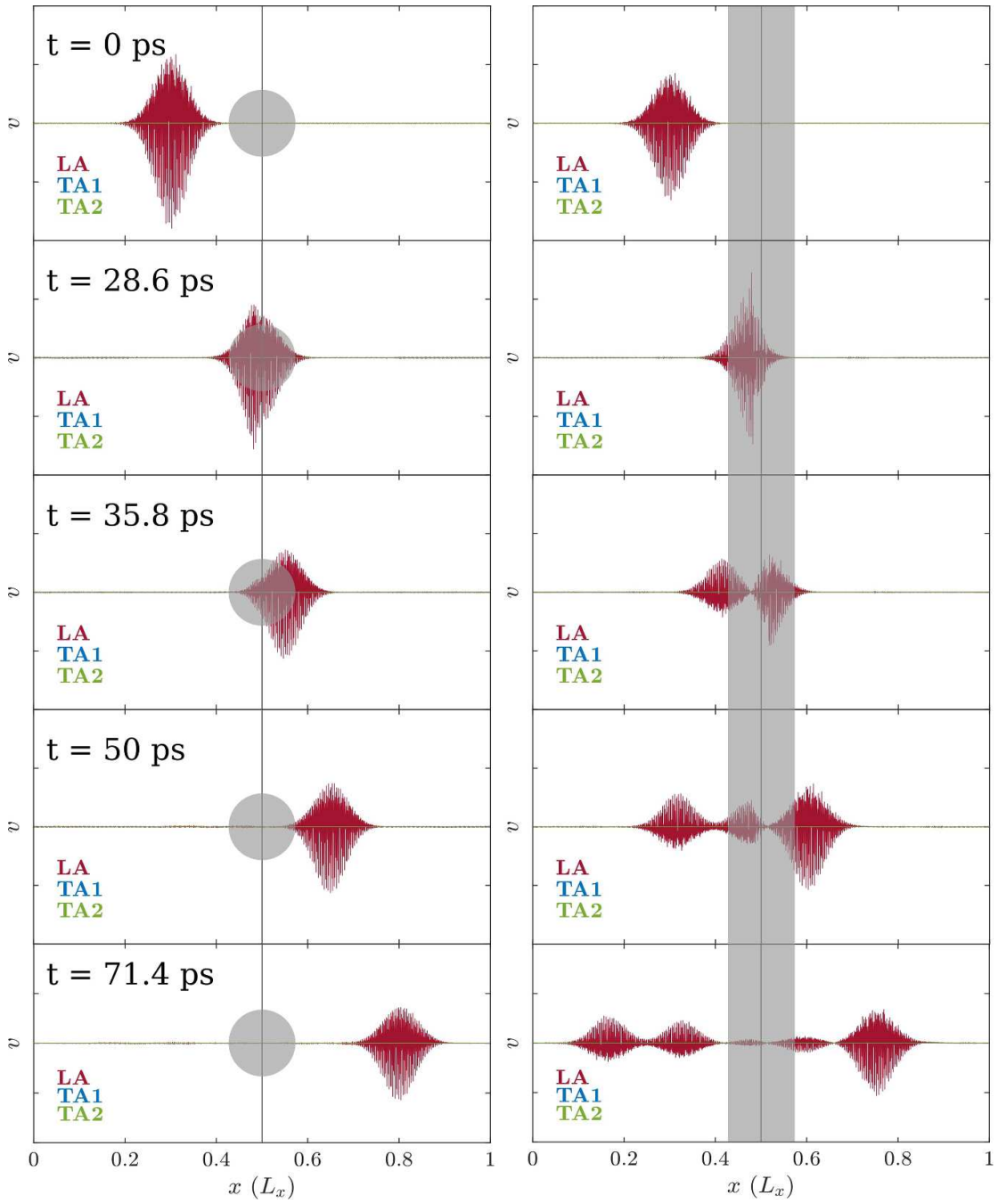

Figure 3. Real-space waveform time evolution for $\gamma = 10.0$—LA mode. Different colors indicate velocities corresponding to the polarization of different modes. The visualization of the nanoparticle and thin slab geometry in the figures are not to scale.

as a function of x in fractional units of L_x in figures 4 and 5 for the incident LA and TA1 mode phonons, respectively.

3.1.2. Results and discussion

First, for the incident LA phonon with $\gamma = 0.15 - 0.5$ (Rayleigh regime), the wave-packet reflection and transmission is qualitatively similar between the nanoparticle and thin slab cases with a distinct single reflected and single transmitted wave-packet. The amplitudes of the residual phonons are relatively comparable, though the transmitted component for the thin slab cases is higher than that of the nanoparticle. The $\gamma = 0.15$ nanoparticle result is more akin to its conjugate thin slab result than the $\gamma = 0.5$ case. Such results are likely a consequence of the incident phonon wavelength being significantly larger than the size of the scatterer, therefore the non-planar geometry of the nanoparticle would only have a minor impact on the wave dynamics. Per this reasoning, the TA1 scattering for γ in the Rayleigh and Mie regimes is expectedly comparable to the LA scattering, however, in the near-Rayleigh to Mie regime cases

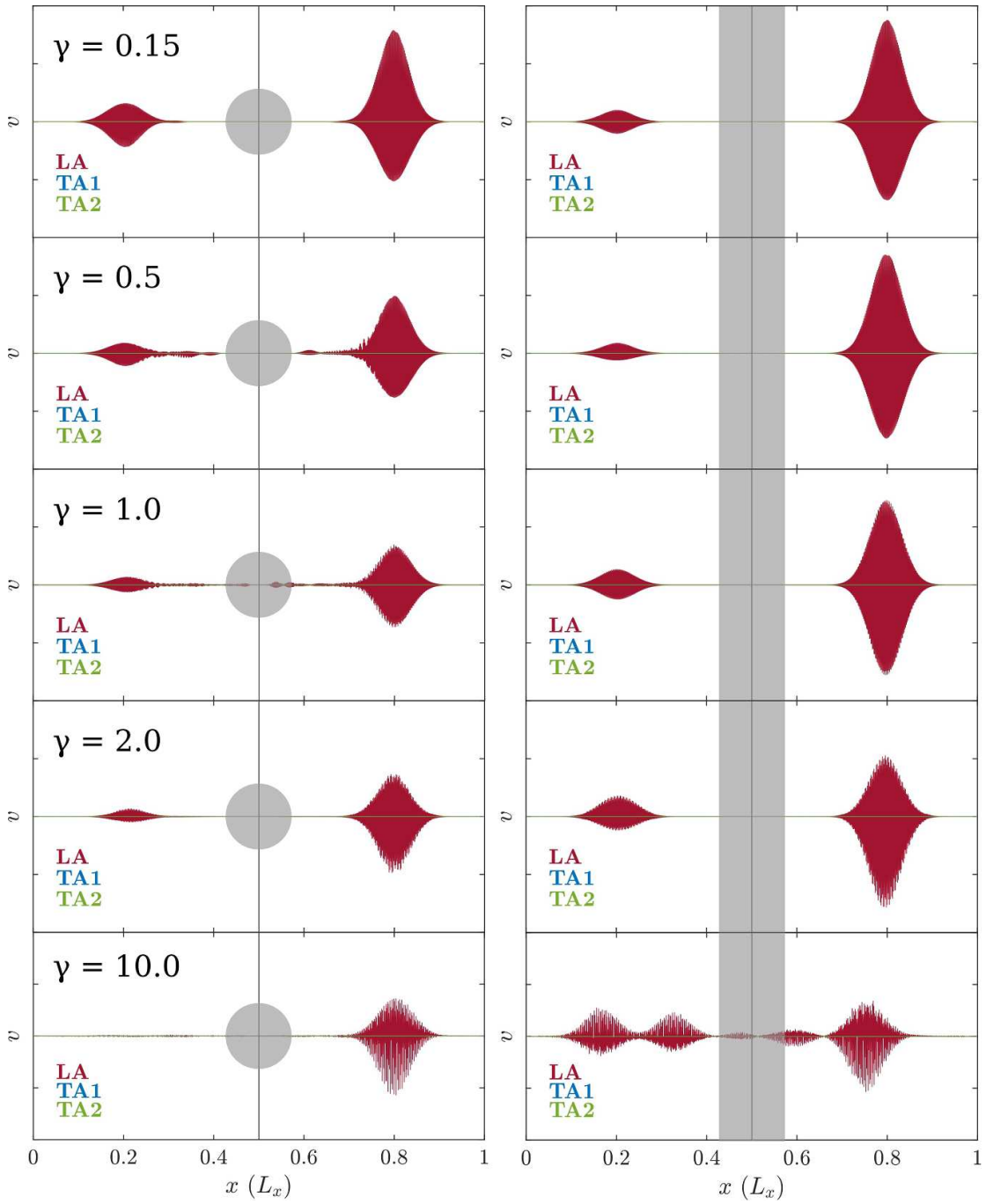

Figure 4. LA mode scattered waveforms at the simulation end. Different colors indicate velocities corresponding to the polarization of different modes. The visualization of the nanoparticle and thin slab geometry in the figures are not to scale.

($\gamma = 0.5 - 2.0$) the nanoparticle excites a vibration in the polarization of the LA mode. The excitation is highly incoherent and approximately propagates with the reflected and transmitted TA1 phonon wave-packets. Similar results were observed for the TA2 phonon-nanoparticle scattering. Since the atom velocities plotted in figures 3–5 are averaged over the y and z directions, it is unclear whether there is also mode conversion in the LA phonon-nanoparticle scattering. Later in section 3.4, we will show there is mode conversion for LA modes in addition to TA1 modes.

As γ is increased up to $\gamma = 2.0$, the scattering between the nanoparticle and thin slab cases is observed to deviate, with the amplitudes of the reflected components in the nanoparticle scattering becoming considerably diminished. For the thin slab, the scatterer size becomes large enough in comparison to λ_0 such that interference of transmitted phonons inside the thin slab occurs and begins to produce multiple reflected WPs as observed in the $\gamma = 2.0$—TA1 simulation. Phonon interference in thin films has been examined in previous literature [29]. Such result is not observed for the nanoparticle case, implying the non-planar

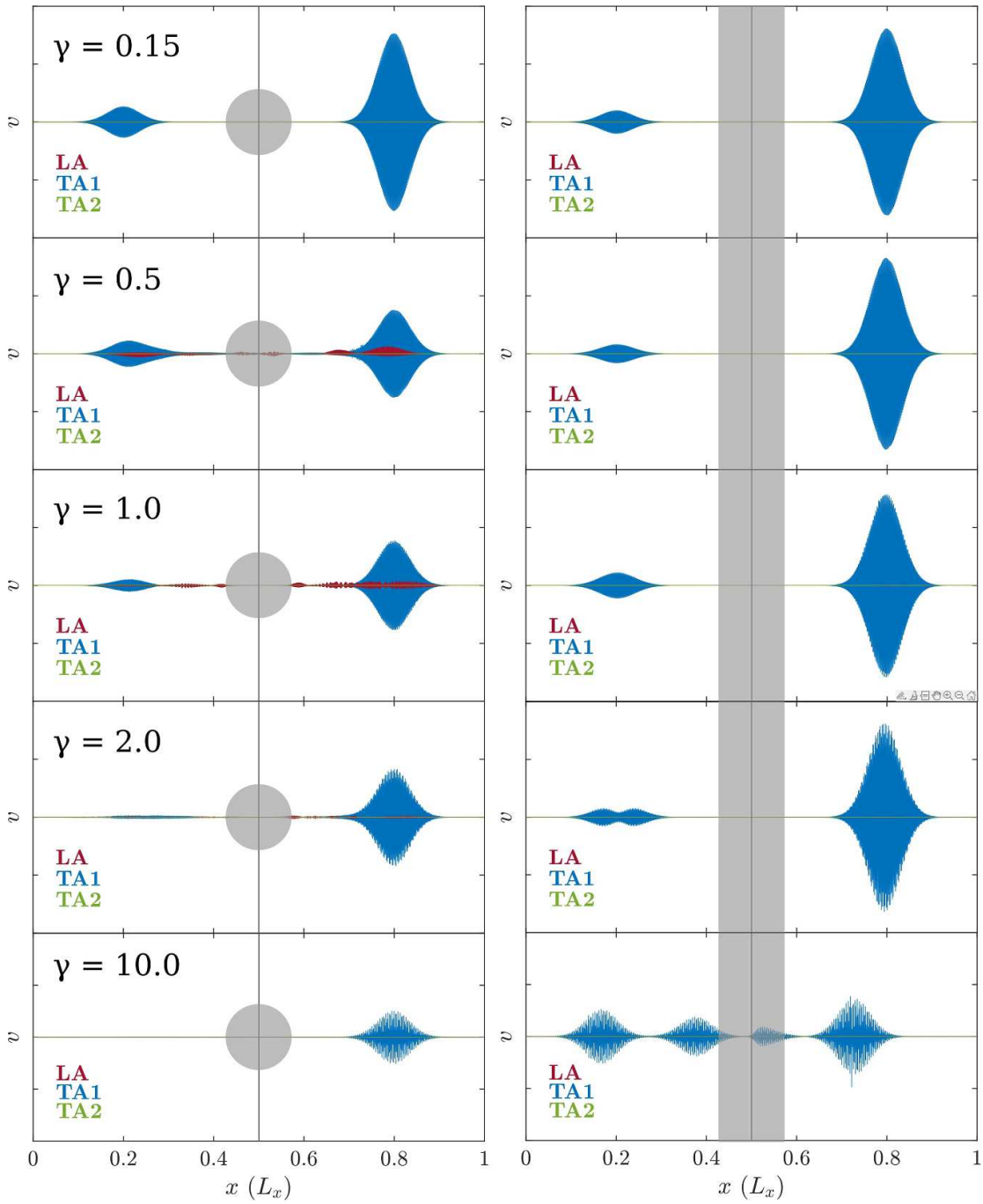

Figure 5. TA1 mode scattered waveforms at the simulation end. A comparable results were observed for the TA2 phonon-nanoparticle scattering. Different colors indicate velocities corresponding to the polarization of different modes. The visualization of the nanoparticle and thin slab geometry in the figures are not to scale.

interfaces impact the state of interference. Particularly, the spherical nanoparticle has a non-uniform thickness where the incident phonon wave-front may interfere strongly along the center-line where the thickness is largest and weakly interfere at the edges where thickness is smallest compared to λ_0. This non-uniformity for the spherical nanoparticle appears to induce destructive interference of the back scattered phonon while only minimally attenuating the amplitude of the transmitted wave. The $\gamma = 10.0$ results, where the range of non-uniformity is magnified, support these conclusions. For both LA and TA1 cases, the thin slab exhibits strong interference producing multiple scattered WPs while the nanoparticle induces no observable reflection. Thus, it is demonstrated that as γ increases into the Geometric regime, the non-planar interfaces yield a non-trivial forward scattering behavior that highly contrasts the scattering dynamics of the planar interfaces. At low γ, the nanoparticle and thin slab scattering are more similar and simulations in the Mie regime ($\gamma = 1.0$) show a transition from Rayleigh to Geometric regime interference behavior.

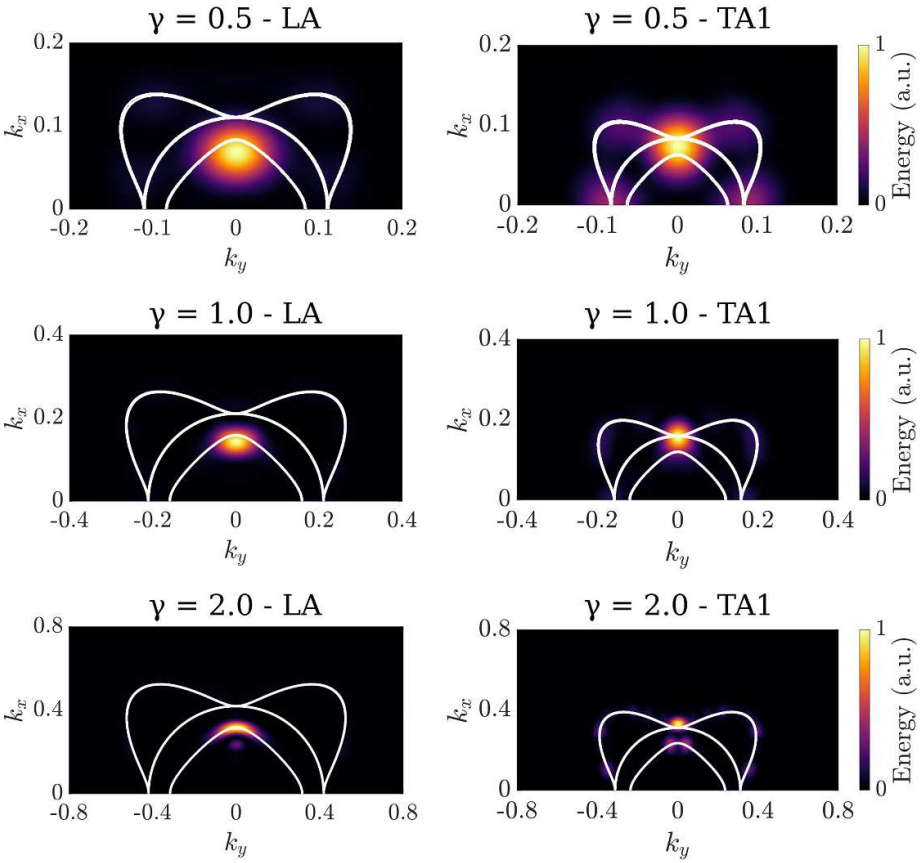

Figure 6. Time-averaged spectral energy density $\langle\Phi\rangle$ for nanoparticle simulations. The white line insets are the iso-frequency lines corresponding to the acoustic modes of the incident phonon frequency ω_0.

In continuum analyses, it is expected that scattering by an interface with curvature larger than the incident wavelength can be approximated as an interaction with a planar interface [30]. Real-space analyses shown here suggest such paraxial approximation is invalid for ballistic phonons approaching the Geometric regime. It is likely that lattice discreteness and anisotropy are the attributing factors for the effects of the non-planar interfaces. Firstly, as evaluated in other interfacial phonon scattering approximations like the AMM and DMM, the comparison between the incident phonon wavelength and surface roughness is significant [2]. At large γ, λ_0 becomes comparable enough to the lattice spacing such that the incident phonon diffusely scatters. In contrast to the planar interfaces of the thin slab, the symmetric curvature of the non-planar interfaces of the spherical nanoparticle is likely altering the path of scattered phonon propagation inside the nanoparticle such that the back-scattered amplitude (of all modes) is attenuated (destructive interference). For low γ, λ_0 is relatively large enough that specular scattering is likely present and the nanoparticle size is insufficiently large to produce strong interference. We examine the validity of these preliminary conclusions in the following sections.

3.2. Energy distribution in reciprocal space

3.2.1. Introduction

In this section, we supplement our analyses of the scattered phonons in real space with a study of the scattered energy distribution in reciprocal space. Previous works applying the phonon wave-packet method such as [31] have been able to provide deep insights into interfacial phonon scattering when real-space analyses are conjoined with reciprocal space calculations.

The spectral energy density Φ associated with a wave-vector $\boldsymbol{k}$ at time t is given as

$$\Phi(\boldsymbol{k},t)=\sum_{x,y,z}^{\alpha}\sum_{i}\frac{M_i}{N}\left|\sum_{m}^{N}v_{i,m}^{\alpha}(t)\exp\left(i\boldsymbol{k}\cdot\boldsymbol{r_0^m}\right)\right|^2 \tag{7}$$

[32]. M_i and $\boldsymbol{r_0^m}$ are the mass and equilibrium position of the ith atom, respectively. The results for the $\gamma=[0.5,1.0,2.0]$ simulations are presented in figure 6 and will now be discussed.

3.2.2. Results and discussion

We first examine the values of $\langle\Phi\rangle$, averaged over the time frame at which the phonon wave-packet passes through the nanoparticle. The resolution in reciprocal space for all computations was kept below $\Delta k = 0.005\frac{2\pi}{a}$. The heat map of the energy density contains an inset of the iso-frequency lines corresponding to the acoustic modes of the incident phonon frequency ω_0. As the wave-packet simulations are conducted with minimal anharmonic interactions, the phonon interaction with the nanoparticle is nearly elastic, therefore it is expected that the spectral energy density peaks will be on the iso-frequency lines. We do not observe this result for the $\gamma = 0.5$ and $\gamma = 1.0$ calculations due to the finite size of the nanoparticle being unable to well-resolve larger wavelengths. There additionally may be an impact of the interfacial phonon modes on the internal vibrations of the nanoparticle at low k_0. Still, the spectral energy density calculations for these simulations provide insights into the orientations of the scattered phonon wave-vector and group velocity.

In all simulations, we observe the energy peak to approximately align along the [100] direction on the iso-frequency line corresponding to the incident phonon mode, with some spreading about this point. This result indicates the scattered phonon propagating through the nanoparticle retains its initial wave-vector and group velocity orientation. We further observe at $\gamma = 0.5$, there is a significant fraction of scattered energy that is present outside the [100] direction, specifically at approximately at $k_x = 0$ and $\phi = \arctan(\frac{k_y}{k_x}) \approx 38^\circ$ on the iso-frequency line corresponding to the TA1 mode. The $k_x = 0$ result indicates that a fraction of the incident TA1 phonon energy is converted into a LA mode with wave-vector and group velocity vector in the orientation of the incident TA1 polarization. The $\phi \approx 38^\circ$ result indicates that the other fraction of mode-converted energy still possess a group velocity orientation that approximately matches the direction of the incident phonon group velocity. The total fraction of mode-converted energy is shown to disappear as γ increases out of the Rayleigh regime.

We find calculation of the scattered phonon energy in reciprocal space uncovers a presence of mode conversion inside the nanoparticle in the near-Rayleigh to Mie regimes, however, the majority of the energy density possesses the group velocity vector orientation of the incident phonon wave. The mode conversion dissipates at higher γ. From this result, we can conclude that the scattering event is nearly one-dimensional for all γ, with most of the reflected and transmitted phonon energy propagating along the axis of the incident group velocity direction. Such result may be a consequence of the quasi-one-dimensional nature of the wave-packet generated, however, it is likely due to the geometric symmetry of the spherical scatterer we simulated. In the following sections, we will uncover and dissect the mechanism behind the mode conversion variation with γ.

3.3. Energy distribution in real space

3.3.1. Introduction

In the previous section, we investigated the distribution of the scattered phonon modes inside the nanoparticle in reciprocal spaces. To obtain further insight into the scattering physics, the energy transport of the phonon wave-packet propagating through the nanoparticle is studied for the first time, in contrast to previous works that have solely looked at the scattered energy outside the nanoparticle in the forms of scattering phase functions [17, 33]. Whereas the spectral energy density calculations in the previous section identified the orientation and polarization of the phonon modes inside the nanoparticle, the plots of the distribution of kinetic energy in real-space identify the actual path and profile of phonon energy propagation. Our analyses of the internal scattered energy reveal a non-trivial 'phonon lensing' effect whereby the non-planar interfaces modify the phonon wave dynamics and resulting transport behaviors. We report and discuss this phenomenon.

3.3.2. Results and discussion

As the spatial width of the ballistic phonon is only specified along the x axis i.e. the [100] direction, the phonon energy of the wave-packet is uniformly spread across the entire yz cross-sectional area. Since periodic boundary conditions are applied to the y and z dimensions, the simulated wave-packet is effectively an infinitely extended plane wave-front. Examining the real-space energy propagation in the xy plane, the wave-packet appears as a collection of lines of constant energy aligned along the y axis. As seen in the real-space waveforms, the thin slab scatters the incident phonon into reflected and transmitted components and these scattered wave-packets still possess a uniform energy distribution over the cross-sectional area. Such results were not observed for the nanoparticle as shown in figures 7 and 8 visualizing the distribution of energy inside the nanoparticle in real-space. We term this distinguishing phenomenon 'phonon lensing' and refer to the characteristic caustics observed in the kinetic energy heat maps as 'lensing structures'.

Upon examining the lensing structures for various γ, qualitative differences are noticeable between low and high γ. From $\gamma = 0.5$ to $\gamma = 1.0$, phonon energy is unevenly focused to various loci inside the

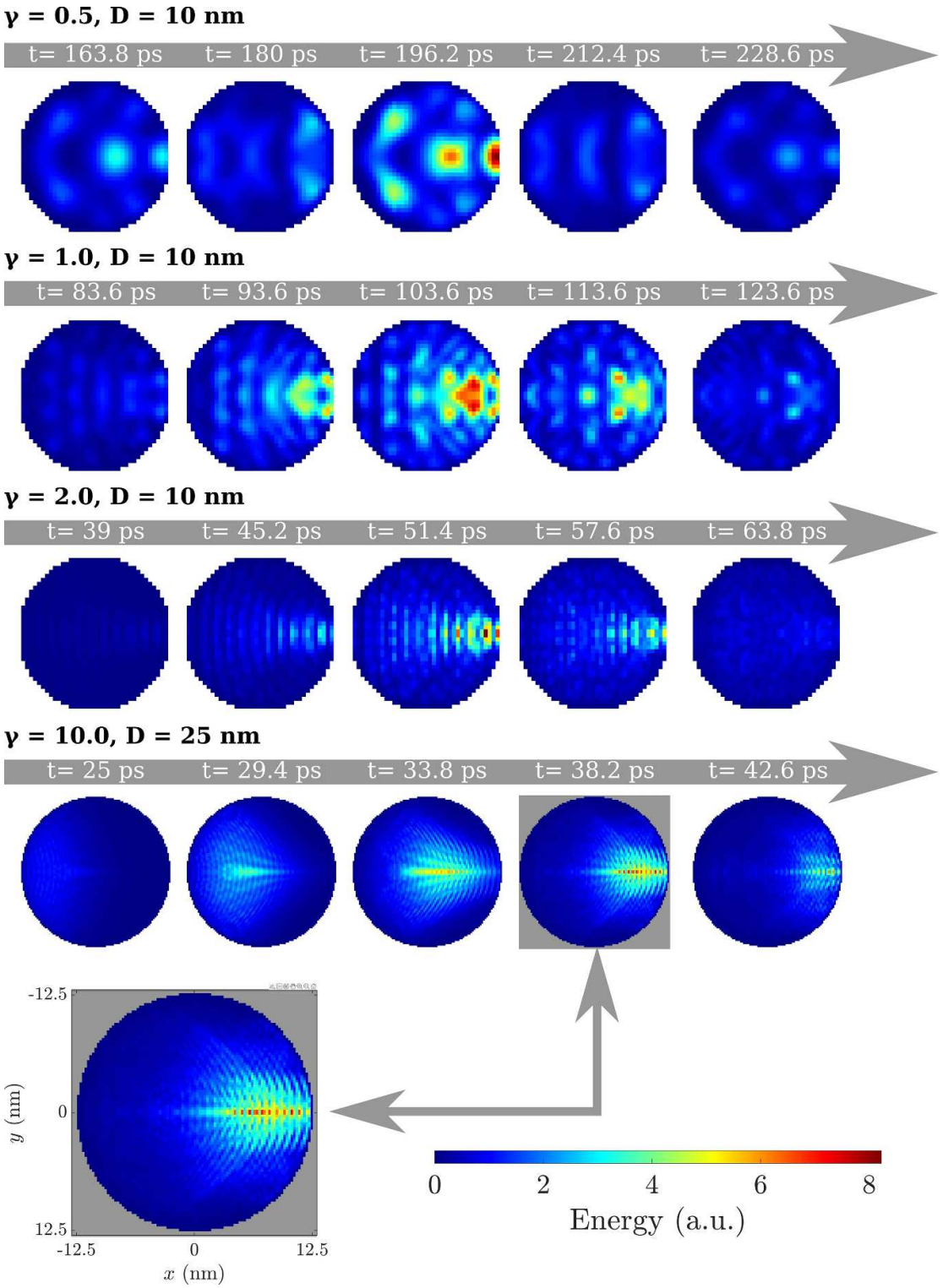

Figure 7. Lensing structures time evolution—LA mode. Lensing is specular at low γ and becomes diffuse at higher γ, as expected by ray-tracing and wave theories of light and other wave-particles.

nanoparticle as the wave-packet passes through with most of the energy concentrated along the center-line parallel to the direction of wave-packet propagation, near the right-most edge of the nanoparticle. The visual appearance of this main focus point motivated the 'phonon lensing' naming scheme. The non-trivial focusing of energy to certain loci inside the nanoparticle is not to be confused with phonon focusing, a separate effect of ballistic phonon transport along certain crystal planes as a result of lattice anisotropy [34]. As γ increases, we see a transition from multiple loci of focused energy to a more diffuse spread of energy inside the nanoparticle. In the case of $\gamma = 2.0$, a single focus point emerges for the LA mode, whereas the TA1

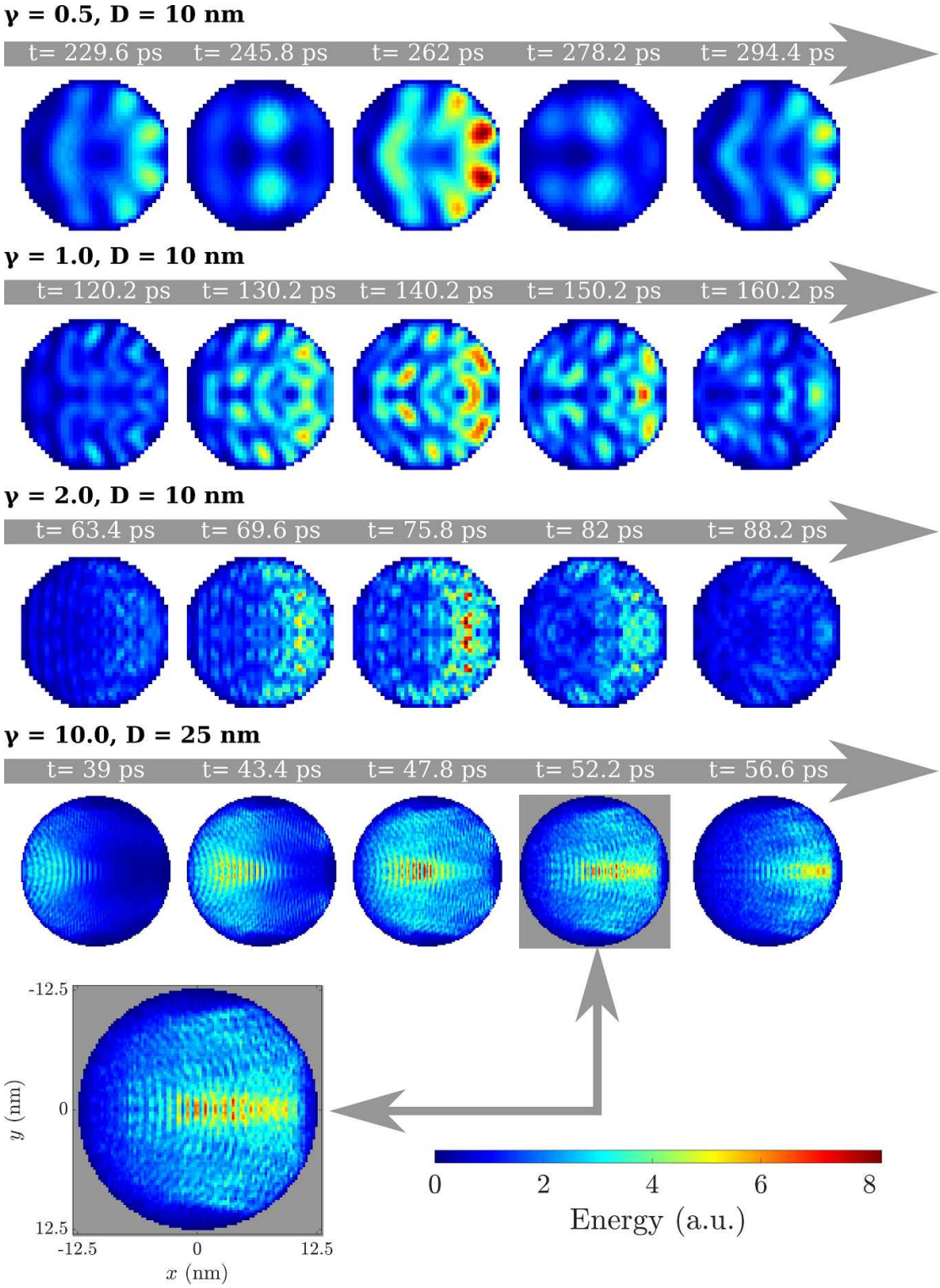

Figure 8. Lensing structures time evolution—TA1 mode. Lensing is specular at low γ and becomes diffuse at higher γ, as expected by ray-tracing and wave theories of light and other wave-particles. Energy is observably more diffuse for lensing of an incident TA1 mode in comparison to the LA mode displayed in figure 7.

mode is significantly defocused. At $\gamma = 10.0$, the single focus point is no longer present and the phonon energy diffusely propagates through the nanoparticle, more so in the TA1 case.

We may think of the phonon lensing effect as a scattering phenomena of phonon waves inside the nanoparticle and the real-space energy distribution results are supportive of the inferences made from the spectral energy density and waveform results in the previous sections. First, we must consider what is fundamentally happening in the scattering interaction. The incident wave must first be refracted by the first non-planar spherical interface that is convex facing the $-x$ direction. At low γ, per the AMM analysis of

scattering, it is expected that the refraction is specular and the propagating phonons may be treated as rays, unaffected by the lattice discreteness. These phonon rays will subsequently reflect and refract at the second non-planar interface that is concave facing the $-x$ direction. The reflected components, under intuitions of light scattering in ray optics, would primarily concentrate in energy at a focal point along the center-line (i.e. the principal axis) near the right most edge of the 'mirror', in this case the concave surface of the nanoparticle interior [30]. We observe this approximate result at low γ and additional loci are likely cause of scattered phonon ray paths meeting, and thus peaking in energy.

The disappearance of multiple focused energy points and uniform spread of energy in the nanoparticle as γ increases out of the Mie regime are supportive of theories of diffuse scattering and interference. As γ increases out of the Mie regime, per the DMM analysis of scattering, the refraction is diffuse and the size of the nanoparticle is large enough in comparison to the phonon wavelength that the scattered waves in the nanoparticle interior have the opportunity to interfere. Thus, the specular scattering is no longer present. We particularly are able to directly observe diffuse caustics in the $\gamma = 2.0$ and 10.0 LA and TA1 cases as the incident wave initially refracts into the nanoparticle. Furthermore, over the time evolution, we see the interference of the energy caustics more prominently in the $\gamma = 10.0$ which matches our predictions based on the scattered waveform results.

3.4. Heat flux and phonon mode conversion

3.4.1. Introduction

In the previous section, it was identified that the path and profile of phonon energy propagation through the nanoparticle is modified by the non-planar interfaces. The observed wave-vector variation of this phonon lensing effect agreed well with our analyses of the wave-vector dependent phonon transmission and reflection. It is of interest to quantify how the states of lensing impact the mode conversion in the scattering event as mentioned in our discussion of the energy distribution in reciprocal space. A key property to which phonon mode conversion is related to is the scattering phase function, which quantifies the angular distribution of scattered energy. Quantification of the scattering phase function then allows computation of the scattering efficiency. Zuckerman and Lukes [17] as well as Kakodkar and Feser [18] have employed the following heat flux expression from [35] to model the energy scattered by the nanoparticle

$$\boldsymbol{J}(t) = \frac{1}{V}\left[\sum_i e_i \boldsymbol{v_i} + \boldsymbol{Q}\right] \tag{8}$$

where $\frac{1}{V}$ is a scaling factor, e_i is the energy of the ith atom and $\boldsymbol{Q}$ is the virial stress term. The scattering phase function is developed from the time-average of equation (8), $\langle \boldsymbol{J} \rangle$. Various expressions for $\boldsymbol{Q}$ have been developed to well-describe virial stress considering two-body and many-body interactions [36]. Conceptually, the first term in equation (8) quantifies the energy transport due to local particle motion which is associated with convection in fluids. We will name this value as the ballistic component. The second term in equation (8), the virial stress $\boldsymbol{Q}$, quantifies the energy dissipation through the work done by interatomic forces. This term, which we will name the diffusive component of the heat flux, is associated with conduction in solids which stems from the atomic stress and the acoustic Poynting vector. A key issue however, in [17, 18], is that the diffusive term is used to compute the scattered energy despite the simulation/calculation being conducted under harmonic conditions. In the harmonic case, there is an absence of anharmonic interactions which arise from the work done by interatomic forces therefore the diffusive component of equation (8) has little conceptual meaning and its value would be insignificant in comparison to the ballistic component. We observed such result for the wave-packet simulations conducted in this work. As an example, in figure 9 we show the mean of each heat flux component as a function of time while the wave-packet passes through the scatterer for the $\gamma = 2.0$—LA nanoparticle simulation.

Due to dominance of the ballistic term, computation of $\boldsymbol{J}$ per-atom only shows the local particle motion and not the magnitude and direction of energy transport. For the case of the thin slab, where there is no lensing and thus no mode conversion, the atoms move along the polarization of the incident mode as seen in figure 10, but the orientation is not representative of the true direction of energy propagation. Still, analysis of the local particle motion offers some qualitative insights into the states of mode conversion as changes in orientation correspond to changes in mode, but not directly the orientation of the wave-vector and group-velocity which is necessary for the scattering phase function calculation. In figure 11, we show heat maps of the time-averaged heat flux orientation $|\theta| = |\arctan(J_y/J_x)|$, effectively the ballistic term, inside the nanoparticle for different mode and γ.

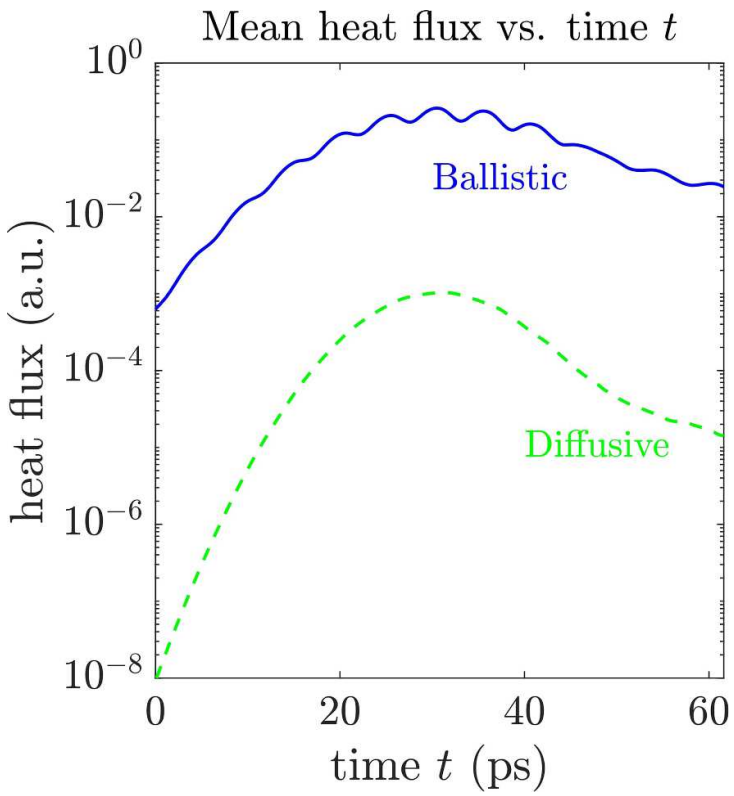

Figure 9. Magnitude comparison of the mean of the ballistic and diffusive components of heat flux in equation (8) as a function of time for the $\gamma = 2.0$—LA nanoparticle simulation. The plot indicates the ballistic term is several orders of magnitude greater than the diffusive term which we argue has been incorrectly used in previous phonon-nanoparticle scattering analyses under harmonic conditions.

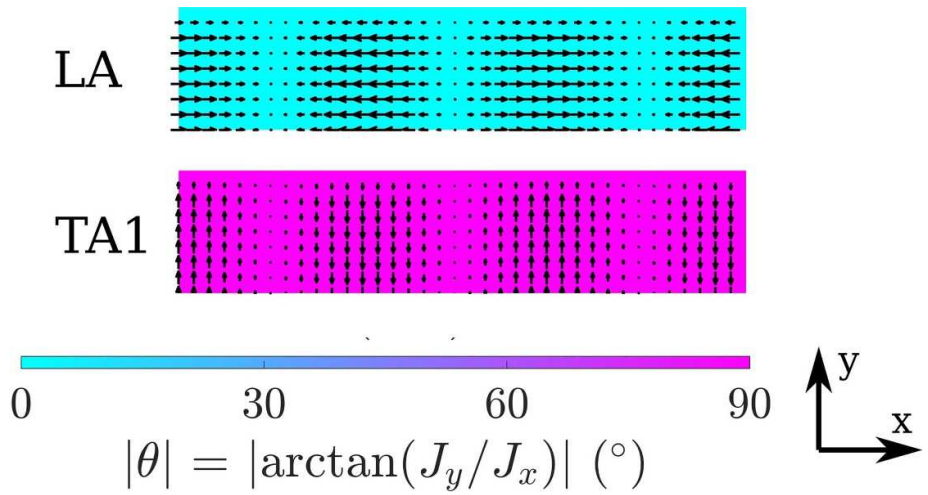

Figure 10. Snapshot of the atomic heat flux magnitude (quiver plot) and orientation (heat map) for the $\gamma = 0.5$ thin slab simulation.

3.4.2. Results and discussion

We find from the heat maps of $|\theta|$ in figure 11, there significant mode conversion towards the outer edges of the nanoparticle, away from the center line. Along the center line where the nanoparticle interface is normal to the incident phonon group velocity, the orientation is nearly unchanged from the polarization of the incident mode, a reasonable result as there is no mode conversion for a flat interfaces as seen for a thin slab in figure 10. Most notably, the observed caustics align well with our dissection of phonon lensing in the previous section. At low γ, there are discrete regions of a single mode and sharp contrasts are present between different regions. This result agrees with the prediction that longer wavelengths scatter through the non-planar interfaces like rays with minimal interference and meet at discrete loci of focused energy. Overall,

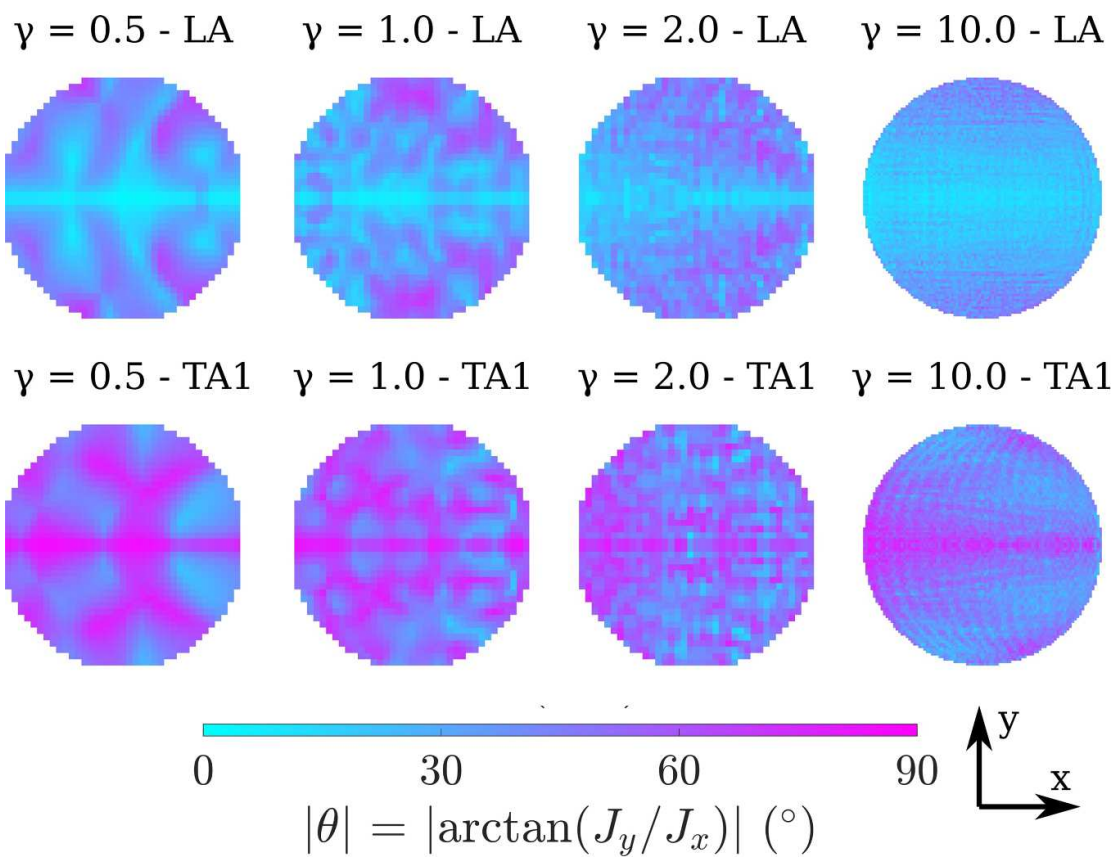

Figure 11. Time-averaged heat flux $\langle \boldsymbol{J} \rangle$ orientation inside the nanoparticle as a function of mode and γ.

there is a distinct structure to the mode conversion profile inside the nanoparticle, which is due to the specularity of the phonon lensing. At larger γ, the mode conversion becomes more incoherent and diffusely spread which is likely owed to the diffuse scattering of phonons and greater wave interference as predicted from the results in the previous sections.

In sum, we showed that the diffusive term of the atomic heat flux employed previous harmonic analyses of phonon-nanoparticle scattering has little conceptual basis when anharmonic interactions are absent, yet the ballistic term is a good proxy for mode conversion analysis. Calculation of the heat flux, effectively the ballistic term, orientation per-atom inside the nanoparticle reveals the state of mode conversion varies with γ in a fashion that is highly consistent with analysis of the phonon lensing effect in the previous section. Specifically, specular interface scattering presumed by AMM holds true under conditions of low γ, whereas the diffuse interface scattering assumption underlying DMM remains applicable in cases of high γ. Furthermore, it is worth noting that these distinct interface scattering behaviors result in varying manifestations of the phonon lensing effect.

4. Conclusions

There is minimal knowledge as to how phonon scatter at non-planar interfaces. This problem is particularly relevant to understanding phonon scattering by embedded nanoparticles which are known to influence thermal transport in a variety of crystalline solids. The MD based phonon wave-packet method is applied to study ballistic phonon wave scattering by a spherical nanoparticle with wave-vector and mode resolution. Identical simulations of the wave-packet incident on a dopant thin slab, a junction of two planar interfaces whereas the nanoparticle is non-planar, were also conducted to compare the scattering between planar and non-planar interfaces. Analysis of the wave dynamics in real and reciprocal spaces reveal non-trivial differences between the nanoparticle and thin slab. Particularly, refraction and reflection of the phonon wave through the non-planar interfaces of the nanoparticle results in a non-trivial 'phonon lensing' effect which alters the path and profile of ballistic phonon energy propagation. This effect is not observed in the thin slab. We explain the lensing dynamics through the ray and wave treatments of phonons and show how the effect impacts the states of mode conversion. Though only the case of a spherical scatterer was examined in this work, it is likely that shape of the scatterer impacts the geometric nature of the lensing and thus the scattering

properties. This work provides a unique dissection into interfacial phonon transport and specifically phonon-nanoparticle scattering. The insights uncovered may be useful in manipulating the paths of heat transfer in phononic systems for enhanced device performance. For instance, they can guide us to design strategies to manipulate the propagation path of lattice heat, reducing thermal conductivity for thermoelectric applications or increasing thermal conductivity towards better heat dissipation in thermal interface materials.

Data availability statement

The data cannot be made publicly available upon publication because no suitable repository exists for hosting data in this field of study. The data that support the findings of this study are available upon reasonable request from the authors.

Acknowledgments

This work is supported by the Nuclear Regulatory Commission (Award No. 31310021M0004) and the National Science Foundation (Award No. 2047109). The authors thank the support of Research & Innovation and the Office of Information Technology at the University of Nevada, Reno for facilitation and access to the Pronghorn High-Performance Computing Cluster.

Credit author statement

Theodore Maranets: Conceptualization, Formal analysis, Software, Writing—Original Draft, Writing—Review and Editing. Yan Wang: Conceptualization, Formal analysis, Supervision, Writing—Original Draft, Writing—Review and Editing.

Conflict of interest

The authors declare that they have no known competing financial interests or personal relationships that could have appeared to influence the work reported in this paper.

ORCID iDs

Theodore Maranets https://orcid.org/0009-0000-4177-3593
Yan Wang https://orcid.org/0000-0001-9474-6396

References

[1] Cahill D G *et al* 2014 Nanoscale thermal transport. II. 2003–2012 *Appl. Phys. Rev.* **1** 011305
[2] Ma T, Chakraborty P, Guo X, Cao L and Wang Y 2020 First-principles modeling of thermal transport in materials: achievements, opportunities and challenges *Int. J. Thermophys.* **41** 1–37
[3] Swartz E T and Pohl R O 1989 Thermal boundary resistance *Rev. Mod. Phys.* **61** 605
[4] Ramiere A, Volz S and Amrit J 2016 Thermal resistance at a solid/superfluid helium interface *Nat. Mater.* **15** 512–6
[5] Hopkins P E and Norris P M 2007 Effects of joint vibrational states on thermal boundary conductance *Nanoscale Microscale Thermophys. Eng.* **11** 247–57
[6] Duda J C, Hopkins P E, Smoyer J L, Bauer M L, English T S, Saltonstall C B and Norris P M 2010 On the assumption of detailed balance in prediction of diffusive transmission probability during interfacial transport *Nanoscale Microscale Thermophys. Eng.* **14** 21–33
[7] Xie R, Tiwari J and Feng T 2022 Impacts of various interfacial nanostructures on spectral phonon thermal boundary conductance *J. Appl. Phys.* **132** 115108
[8] Kim W, Zide J, Gossard A, Klenov D, Stemmer S, Shakouri A and Majumdar A 2006 Thermal conductivity reduction and thermoelectric figure of merit increase by embedding nanoparticles in crystalline semiconductors *Phys. Rev. Lett.* **96** 045901
[9] Luckyanova M N *et al* 2018 Phonon localization in heat conduction *Sci. Adv.* **4** eaat9460
[10] Coetzee D, Venkataraman M, Militky J and Petru M 2020 Influence of nanoparticles on thermal and electrical conductivity of composites *Polymers* **12** 742
[11] Majumdar A S M E 1993 Microscale heat conduction in dielectric thin films *J. Heat Transfer* **115** 7–16
[12] Kim W and Majumdar A 2006 Phonon scattering cross section of polydispersed spherical nanoparticles *J. Appl. Phys.* **99** 084306
[13] Prasher R S 2004 Thermal transport cross section and phase function of longitudinal phonons for scattering by nanoparticles and microparticles *J. Appl. Phys.* **96** 5202–11
[14] Feser J P 2019 Engineering heat transport in nanoparticle-in-alloy composites: the role of Mie scattering *J. Appl. Phys.* **125** 145103
[15] Tian Z, Esfarjani K, Shiomi J, Henry A S and Chen G 2011 On the importance of optical phonons to thermal conductivity in nanostructures *Appl. Phys. Lett.* **99** 053122
[16] Kundu A, Mingo N, Broido D A and Stewart D A 2011 Role of light and heavy embedded nanoparticles on the thermal conductivity of SiGe alloys *Phys. Rev.* B **84** 125426

[17] Zuckerman N and Lukes J R 2008 Acoustic phonon scattering from particles embedded in an anisotropic medium: a molecular dynamics study *Phys. Rev.* B **77** 094302
[18] Kakodkar R R and Feser J P 2018 Wavevector and polarization resolved analysis of phonon scattering from embedded nanoparticles *J. Appl. Phys.* **124** 085107
[19] Kakodkar R R and Feser J P 2015 A framework for solving atomistic phonon-structure scattering problems in the frequency domain using perfectly matched layer boundaries *J. Appl. Phys.* **118** 094301
[20] McGaughey A J H and Kaviany M 2006 Phonon transport in molecular dynamics simulations: formulation and thermal conductivity prediction *Adv. Heat Transfer* **39** 169–255
[21] Hanus R, Gurunathan R, Lindsay L, Agne M T, Shi J, Graham S and Snyder G J 2021 Thermal transport in defective and disordered materials *Appl. Phys. Rev.* **8** 031311
[22] Schelling P K, Phillpot S R and Keblinski P 2002 Phonon wave-packet dynamics at semiconductor interfaces by molecular-dynamics simulation *Appl. Phys. Lett.* **80** 2484–6
[23] Huberman S C, Larkin J M, McGaughey A J H and Amon C H 2013 Disruption of superlattice phonons by interfacial mixing *Phys. Rev.* B **88** 155311
[24] Landry E S, Hussein M I and McGaughey A J H 2008 Complex superlattice unit cell designs for reduced thermal conductivity *Phys. Rev.* B **77** 184302
[25] Wang Y, Huang H and Ruan X 2014 Decomposition of coherent and incoherent phonon conduction in superlattices and random multilayers *Phys. Rev.* B **90** 165406
[26] Wang Y, Gu C and Ruan X 2015 Optimization of the random multilayer structure to break the random-alloy limit of thermal conductivity *Appl. Phys. Lett.* **106** 073104
[27] Abeles B 1963 Lattice thermal conductivity of disordered semiconductor alloys at high temperatures *Phys. Rev.* **131** 1906
[28] Thompson A P *et al* 2022 Lammps-a flexible simulation tool for particle-based materials modeling at the atomic, meso and continuum scales *Comput. Phys. Commun.* **271** 108171
[29] Chen G 1999 Phonon wave heat conduction in thin films and superlattices *J. Heat Transfer* **121** 945-953
[30] Hecht E 2012 *Optics* (Pearson Education India)
[31] Shao C, Rong Q, Li N and Bao H 2018 Understanding the mechanism of diffuse phonon scattering at disordered surfaces by atomistic wave-packet investigation *Phys. Rev.* B **98** 155418
[32] Feng T, Qiu B and Ruan X 2015 Anharmonicity and necessity of phonon eigenvectors in the phonon normal mode analysis *J. Appl. Phys.* **117** 195102
[33] Chowdhury O and Feser J P 2022 Phonon scattering and vibrational localization in 2d embedded nanoparticle composites *J. Appl. Phys.* **131** 194301
[34] Wolfe J P 1998 *Imaging Phonons* (Cambridge University Press)
[35] Volz S and Chen G 1999 Lattice dynamic simulation of silicon thermal conductivity *Physica* B **263** 709–12
[36] Surblys D, Matsubara H, Kikugawa G and Ohara T 2019 Application of atomic stress to compute heat flux via molecular dynamics for systems with many-body interactions *Phys. Rev.* E **99** 051301